PAPER

Potential energy curve for $B^1\Pi$ state of $^{85}Rb^{133}Cs$ obtained via genetic algorithm

Physica Scripta

PAPER

Potential energy curve for $B^1\Pi$ state of $^{85}Rb^{133}Cs$ obtained via genetic algorithm

RECEIVED
4 January 2024

REVISED
8 February 2024

ACCEPTED FOR PUBLICATION
20 February 2024

PUBLISHED
4 March 2024

Yide Yin[1], **Ziang Li**[1], **Xuhui Bai**[1], **Ting Gong**[2], **Zhonghua Ji**[3], **Yanting Zhao**[3], **Yongchang Han**[1], **Jie Yu**[1,*] **and Gaoren Wang**[1,*]

[1] School of Physics, Dalian University of Technology, Dalian 116024, People's Republic of China
[2] School of Applied Science, Taiyuan University of Science and Technology, Taiyuan 030024, People's Republic of China
[3] State Key Laboratory of Quantum Optics and Quantum Optics Devices, Institute of Laser Spectroscopy, Shanxi University, Taiyuan 030006, People's Republic of China
[*] Authors to whom any correspondence should be addressed.

E-mail: yujie@dlut.edu.cn **and** gaoren.wang@dlut.edu.cn

Keywords: potential energy curve, $^{85}Rb^{133}Cs$ molecule, genetic algorithm

Supplementary material for this article is available online

Abstract

We adopt the genetic algorithm to fit the potential energy curve for $B^1\Pi$ state of $^{85}Rb^{133}Cs$ molecule based on the data of rovibrational energy levels, which were observed previously by Fourier-transform spectroscopy and photoassociation spectroscopy. We explore the effect of different hyperparameter settings on the evolutionary process and final results to optimise the performance of the algorithm. Finally, the fitting procedure can reproduce the rovibrational levels with an error less than 0.06 cm^{-1} compared to the experimental data.

1. Introduction

During the past twenty years, there has been an increasing interest from both physicists and chemists in the cold and ultracold molecules, especially the polar molecules, since such molecules hold promise for various fields, such as ultracold chemistry, testing fundamental laws, and quantum computing [1]. Several kinds of ultracold polar molecules have been produced successfully through methods such as photoassociation [2] or magnetoassociation [3]. Among these species, the RbCs molecule is fascinating for its unique features [4]. Earlier in this century, Kerman *et al* produced $^{85}Rb^{133}Cs$ molecules in the lowest triplet state $a^3\Sigma^+$ via photoassociation in a laser-cooled mixture of ^{85}Rb and ^{133}Cs atoms [5]. Since then, progress on producing the RbCs molecules via photoassociation has been accomplished [6–8]. Recently, the production of $^{85}Rb^{133}Cs$ molecules in the ground electronic state $X^1\Sigma^+$ has been achieved [9, 10].

For investigating and manipulating the process of photoassociation, potential energy curves (PEC) of different electronic states are of great significance. With precise PEC, accurate rovibrational wave functions and Frank–Condon factors can be calculated, which can be used to fit the photoassociation spectrum [11]. Besides, precise PEC is vital for accurate numerical simulation of the photoassociation process, facilitating the exploration of efficient photoassociation pathways [12–14]. The PEC for the lowest $^1\Pi$ state, namely $B^1\Pi$ state, has been studied extensively. Through the *ab initio* calculations, the PEC for $B^1\Pi$ state of $^{85}Rb^{133}Cs$ molucule has been calculated in [15–19]. Alternatively, techniques that transform rovibrational and hyperfine spectroscopic data into molecular PEC have also been developed, including the Rydberg-Klein-Rees method [20–24] and the inverted perturbation approach (IPA) [25, 26]. Adopting the IPA, Birzniece *et al* constructed an empirical PEC for $B^1\Pi$ state with the rovibrational levels observed by Fourier-transform spectroscopy (FTS) [27]. Recently, additional rovibrational levels of $B^1\Pi$ state have been observed based on photoassociation spectroscopy (PAS) in [10]. However, neither the *ab initio* PEC nor the empirical PEC in [27] can precisely describe the experimentally observed energy levels in [10].

Therefore, the main goal of the present study is to obtain a PEC for $B^1\Pi$ state of $^{85}Rb^{133}Cs$ by taking the rovibrational energy levels observed via both FTS and PAS into account. The empirical PEC in [27] exhibits a bump-like region. Similar irregular shape of the PEC, such as the double-well structure [28–31], are widely available. In order to fit such kind of PEC, it is essential to use more flexible optimisation method. Thanks to the development of computing technology, lots of new techniques for fitting PEC with spectroscopic data have been developed, such as neural networks [28, 32–34] and genetic algorithm (GA) [31, 35–39]. Roncaratti *et al* first proposed a GA technique to fit the analytical PEC for the H_2^+ and Li_2 systems [35]. Marques *et al* proposed a two-step GA using an extended-Rydberg potential and used it on the NaLi and Ar_2 [36]. Almeida *et al* improved the algorithm from [36] to fit the PEC of RbCs ground electronic state [37]. Stevenson *et al* developed a GA approach to fit the point-wise potential directly and adopted it on the $X^1\Sigma^+$ state of LiRb [38, 39]. Urbańczyk *et al* applied GA to fit the double-well PEC for the $E^3\Sigma_1^+$ state of CdKr and CdAr [31]. Inspired by these work, we adopt GA to fit the PEC for $B^1\Pi$ state of $^{85}Rb^{133}Cs$ molecules, in the hope of getting a satisfactory result.

The remaining part of this article proceeds as follows: the second section introduces the methodology used in the present study; the third section presents the fitting results and analyses; the last section states the conclusion of the present study.

2. Methods

GA is a classical and powerful optimisation algorithm inspired by natural selection [40]. It is widely used for solving complex problems, which require extensive parameter space exploration. At first, it creates an initial population of candidate solutions for the problem at hand. It then applies the process of selection, crossover, and mutation to evolve the population. During each generation, the algorithm evaluates the fitness of each candidate solution, selects the better solutions, and recombines them through the crossover to create new solutions. These new solutions are then mutated to introduce minor changes to their parameters. This process is iterated for hosts of generations. As a result, the algorithm can find optimal solutions to the problem. The flowchart of our algorithm is shown in figure 1. Each process in this flowchart is clarified in the next subsections.

2.1. Encoding scheme

The encoding scheme plays a vital role in GA. Generally, we need to choose different encoding schemes according to the properties of different problems. Typical encoding schemes in GA include binary, permutation, and value-based encoding [41]. In the present study, we adopt a value-based encoding scheme that is detailed below.

The fitting is based on the empirical PEC obtained in [27], as shown in figure 2. There are 27 points in this point-wise PEC. In this work, the minimum of the PEC of the ground electronic state is set to be the zero point of energy. As indicated by red shadowed area in figure 2, the energy range of the rovibrational levels observed via PAS is between 13 884 cm^{-1} and 14 149 cm^{-1}, which is covered by the 7th to 19th potential points as noted by the coloured points. These 13 points are adjusted to precisely fit the experimental data.

We firstly estimate the adjustment range of the horizontal and vertical coordinates for all potential points. We calculate the energies of rovibrational levels observed via PAS using the empirical PEC in [27] and compare these calculated energies with their corresponding experimental values in [10]. The errors between them are within 5 cm^{-1}, as listed in table A1. Therefore, the adjustment range of the vertical coordinates for most of the potential points is set to be 15 cm^{-1}, which is several times larger than 5 cm^{-1} and ensures a relatively large search space. Besides, the difference in internuclear distances between the neighbouring potential points is about 0.1 Å, so the adjustment range of the horizontal coordinates for most of the potential points is set to be 0.02 Å, which is several times less than 0.1 Å and ensures a proper shape of the PEC. The adjustment range for the potential points satisfing the case above is noted by the green boxes in figure 2. However, there are exceptions for two groups of points. Firstly, there is a bump-like region covered by the 8th, 9th and 10th points, which is caused by the spin–orbit coupling with the $\Omega = 1$ component of the $c^3\Sigma^+$ state. Therefore, we set a larger adjustment range for these 3 points one by one to expand the search space, as noted by the blue boxes in figure 2. Secondly, for the 12th, 13th and 14th points located at the bottom of the potential well, we mainly focus on adjusting their horizontal coordinates to adjust the equilibrium internuclear distance, as noted by the red boxes in figure 2. The adjustment ranges for each point are listed in table 1.

We generate 26 random numbers distributed uniformly across the adjustment ranges mentioned above. These 26 random numbers make up an individual in the population, and each number represents a gene in this individual. We repeat this process N times to create the initial population. In the present study, we set $N = 200$, meaning there are 200 individuals in the population.

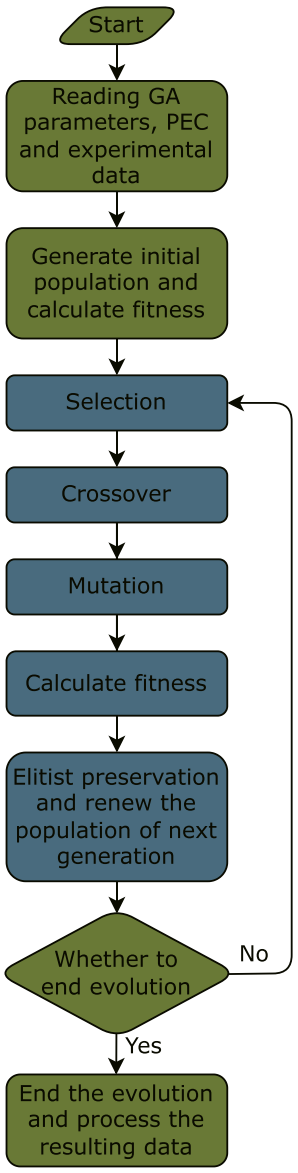

Figure 1. The flowchart of the algorithm adopted in this work.

2.2. Fitness function

After creating the initial population, we need to define the fitness function that measures the performance of individuals. On the one hand, there are 15 rovibrational levels in our fitting, which are observed by PAS in [10] and listed in table A1. On the other hand, a wealth of rovibrational levels are observed by FTS in [27]. We determine the energy levels included in the fitting based on the following considerations. Firstly, the energy range of the rovibrational levels observed by FTS, which are included in our fitting, should be comparable to that observed by PAS. Secondly, part of the energy levels observed by FTS are perturbed by rovibrational levels belonging to the neighbouring electronic state, which is indicated by the deviation of the rotational constant from its conventional value [27]. We choose the rovibrational levels which are free of perturbation. Due to the above considerations, we pick 50 energy levels with $v = 0, 1, 2$ observed by FTS, which are listed in tables A2 and A3. In total, there are 65 energy levels being used in the fitting, and the energies of these rovibrational levels observed experimentally are denoted as $E_{\rm obs}$.

To calculate the fitness for each individual, we firstly add the adjustment values, namely the genes in the individual, to the initial PEC. Then we perform the cubic spline interpolation on these points and obtain a continuously derivable PEC. We solve the corresponding time-independent Schrödinger equation to calculate the energies of rovibrational levels with a Fortran program LEVEL [42]. The fitness function is given by the following equations. Firstly, the mean squared error (MSE) between the calculated energies of rovibrational levels and the corresponding FTS data is

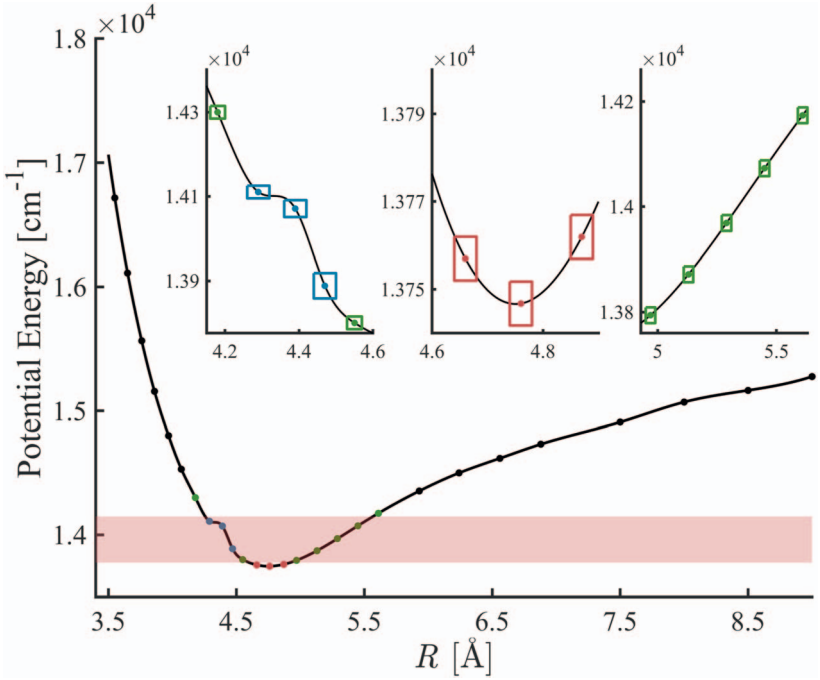

Figure 2. The PEC for $B^1\Pi$ state of $^{85}Rb^{133}Cs$ taken from [27]. The red shadowed area in the main figure indicates the energy range of rovibrational levels observed via PAS. The coloured boxes in the subfigures show the adjustment ranges of the potential points in the fitting procedure. Note that the scales of the vertical axis in subfigures are different.

Table 1. The point-wise PEC for $B^1\Pi$ state of $^{85}Rb^{133}Cs$. Note that only the adjusted points are listed in this table. The first two columns are the original values in [27], the next two columns are the values fitted by GA, and the last two columns are the adjustment ranges for each point.

R [Å]	E [cm^{-1}]	R [Å]	E [cm^{-1}]	ΔR [Å]	ΔE [cm^{-1}]
4.18	14 299.836	4.1851	14 298.4121	(−0.02, 0.02)	(−15, 15)
4.29	14 110.440	4.2650	14 116.3740	(−0.03, 0.03)	(−15, 15)
4.39	14 071.068	4.4116	14 073.4572	(−0.03, 0.03)	(−20, 20)
4.47	13 888.589	4.4651	13 914.6807	(−0.03, 0.03)	(−30, 30)
4.55	13 800.746	4.5445	13 803.5499	(−0.02, 0.02)	(−15, 15)
4.66	13 756.971	4.6775	13 753.8804	(−0.02, 0.02)	(−5, 5)
4.76	13 746.751	4.7558	13 746.4218	(−0.02, 0.02)	(−5, 5)
4.87	13 761.915	4.8824	13 765.3732	(−0.02, 0.02)	(−5, 5)
4.97	13 794.050	4.9857	13 800.1981	(−0.02, 0.02)	(−15, 15)
5.13	13 871.758	5.1299	13 872.5850	(−0.02, 0.02)	(−15, 15)
5.29	13 969.069	5.2949	13 971.0506	(−0.02, 0.02)	(−15, 15)
5.45	14 073.051	5.4633	14 072.9447	(−0.02, 0.02)	(−15, 15)
5.61	14 173.995	5.5997	14 187.7000	(−0.02, 0.02)	(−15, 15)

$$\chi^2_{\rm FT} = \frac{1}{N_{\rm FT}}\sum_{v,J}[E^{\rm FT}_{\rm cal}(v,J) - E^{\rm FT}_{\rm obs}(v,J)]^2, \tag{1}$$

and the MSE for PAS data is

$$\chi^2_{\rm PA} = \frac{1}{N_{\rm PA}}\sum_{v,J}[E^{\rm PA}_{\rm cal}(v,J) - E^{\rm PA}_{\rm obs}(v,J)]^2. \tag{2}$$

In these two equations, $E^{\rm FT}_{\rm obs}$ and $E^{\rm PA}_{\rm obs}$ are the energies of rovibrational levels observed via FTS and PAS, respectively. $E^{\rm FT}_{\rm cal}$ and $E^{\rm PA}_{\rm cal}$ are the calculated energies of these levels. $N_{\rm FT}$ and $N_{\rm PA}$ are the numbers of these energy levels considered in the fitting. The fitness function of an individual is defined as

$$\chi^2 = (1 - W)\chi^2_{\rm FT} + W\chi^2_{\rm PA}, \tag{3}$$

where W is the fitness weight, which denotes the weight of energy levels observed by PAS in the fitting, and takes the value between 0 and 1.

2.3. Operators

After calculating the fitness of the initial population, we need to generate a new population for the next generation. It usually needs the operators including selection, crossover and mutation for general GA to achieve this. The operators adopted in our algorithm are described in the following.

To begin with, we should select the individuals with better fitness from the current population. There are various selection techniques, such as roulette-wheel, tournament, linear-rank, and elite selection [41, 43]. In the present study, we choose the tournament selection described as follows. Firstly, we randomly select n individuals from the current population, where $n = \sigma_s N$ and σ_s denotes the selecting proportion. From these individuals, we select the one with best fitness. We repeat the above process N times and select N individuals to compose the new population.

We then need to cross these individuals in the current population. There are hosts of crossover operators such as single-point crossover, two and k-point crossover [41]. Because the encoding scheme in the present study is relatively simple, only a simplified single-point crossover operator is adopted in the algorithm. For each step of the crossover operation, we randomly select two individuals in the population. The crossing probability of these two individuals is set to be P_c. If the crossover occurs, we should swap the genes at a randomly picked location in the two individuals. If not, we move straight to the next step. We repeat the above step N times in a complete crossover operation.

After that, we need to mutate the individuals in the current population. Since we adopt the real number encoding scheme in the present study, we choose an improved non-uniform mutation operator [44] in the fitting. We first randomly pick a gene in a randomly picked individual. The mutating probability of this gene is set to be P_m. If the mutation occurs, we should add a random number Δ to the current value. For the normal case, Δ is defined as

$$\Delta = \begin{cases} r(V_c - V_{\min})\left(1 - \dfrac{t}{T}\right)^2, & r \leqslant 0 \\ r(V_{\max} - V_c)\left(1 - \dfrac{t}{T}\right)^2, & r > 0 \end{cases} \tag{4}$$

where r is a uniform random number between -1 and 1, V_c is the value of the current gene, $V_{\max}$ and $V_{\min}$ is the upper and lower boundary of adjustment range of this gene, t is the current generation number, and T is the maximal generation number of the whole evolution. If the mutation does not occur, we proceed directly to the next step. As indicated in equation (4), the values of genes can move freely across the parameter space in early generations of evolution, which can contribute to increase population diversity. As evolution proceeds, Δ adaptively diminishes, so it becomes a local search later in the evolution. To avoid falling into local minima, we introduced the possibility of strong mutation on the premise of normal mutation. If the best fitness of the population hasn't improved in 5 consecutive generations, the strong mutation might be activated. The strong mutating probability is denoted by P_s. If the strong mutation occurs, Δ should take the following form,

$$\Delta = \begin{cases} r(V_c - V_{\min})\left(\dfrac{t}{T}\right)^2, & r \leqslant 0 \\ r(V_{\max} - V_c)\left(\dfrac{t}{T}\right)^2, & r > 0 \end{cases} \tag{5}$$

which is helpful to explore a wider range of possible solutions. If not, Δ still takes the form in equation (4). The flowchart for one step of the mutation operation is shown in figure 3. In a whole mutation operation, we repeat the above step 5200 times, since there are 26 genes in an individual and 200 individuals in the population. Therefore, the mutation is a more enhanced operation in comparison to the crossover.

Furthermore, we adopt the elitist preservation strategy to guarantee global convergence. After completing the selection, crossover and mutation operations for the current generation, this strategy directly copy the best individual that has emerged in the evolution so far, replacing the worst individual in the current population. In the present work, we set $T = 200$, repeatedly iterate the process above T times throughout the entire GA procedure and complete the evolution.

3. Results

To optimise the GA procedure, we explored the influence of the hyperparameters in our algorithm on the evolutionary process and final results. These hyperparameters include the fitness weight W, mutating probability P_m, crossing probability P_c, strong mutating probability P_s and selecting proportion σ_s, which have been introduced above. Considering the results of GA are stochastic, we repeatedly executed the GA procedure

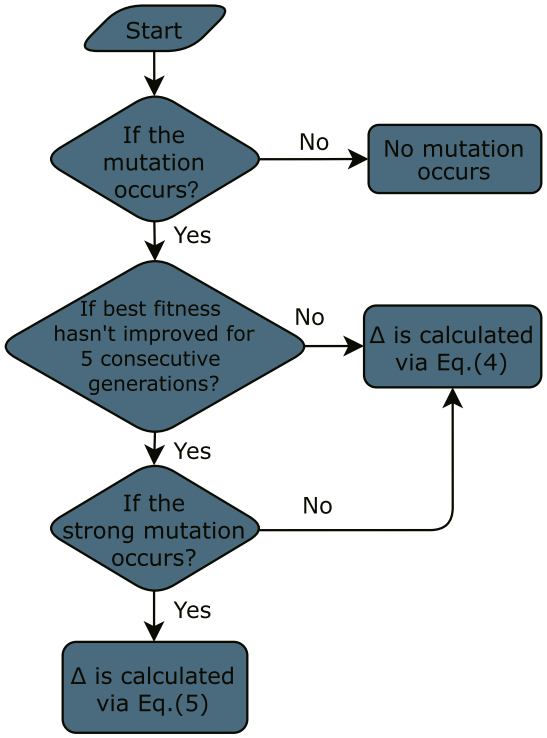

Figure 3. The flowchart of one step in the mutation operation.

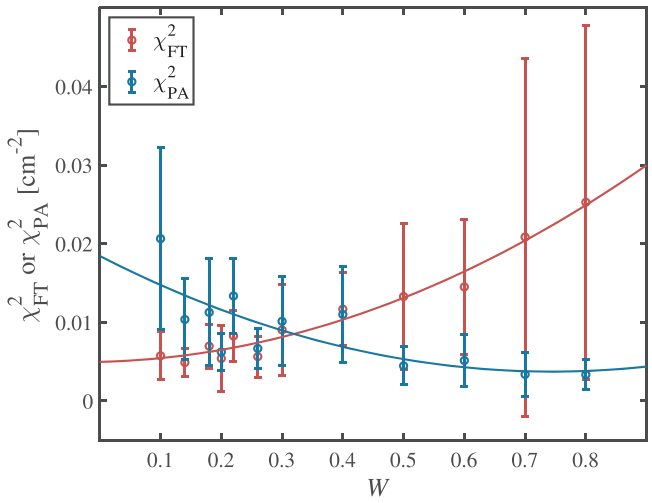

Figure 4. The variations of final χ^2_{FT} and χ^2_{PA} as a function of W, with $P_m = 1$, $P_c = 0.2$, $P_s = 0.2$ and σ_s=0.4. The hollow circles and the error bars represent the average values and the standard deviations. The solid lines fit χ^2_{FT} and χ^2_{PA} as a function of W with the quadratic polynomial.

10 times for each setting of hyperparameters, and the average values and standard deviations are calculated and shown in the following.

We firstly investigate the effect of W in the fitness function on the final results. Since our purpose is to fit a PEC for describing the energy levels observed by both PAS and FTS, it is essential to set the fitness weight W properly to ensure that both χ^2_{FT} and χ^2_{PA} are down to a small value in the end. Fixing other hyperparameters, we change the value of W from 0.1 to 0.8 in a step length of 0.1 and run the GA procedure 10 times for each setting. After obtaining the final χ^2_{FT} and χ^2_{PA} at the end of the evolution of these 10 trials, we calculate their average value and standard deviation as shown in figure 4. The solid lines in figure 4 depict the fitting of χ^2_{FT} and χ^2_{PA} as a function of W with the quadratic polynomial. Since W represents the weight of energy levels observed by PAS in

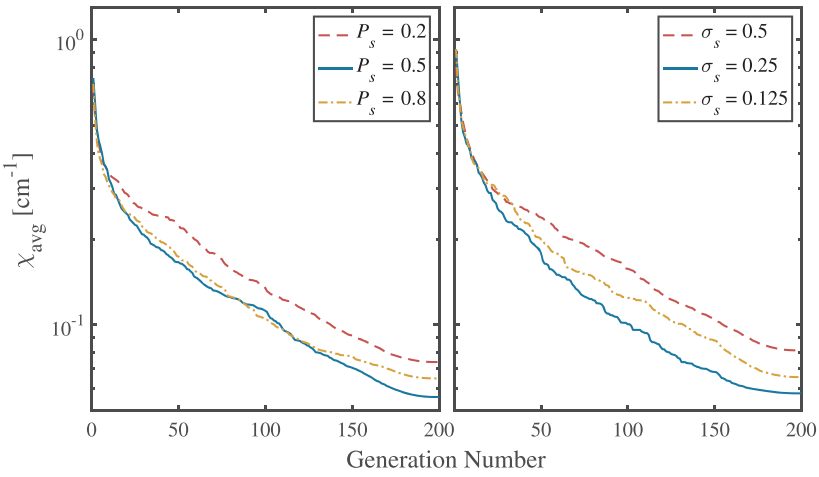

Figure 5. The variations of χ_{avg} as a function of generation number for different P_s with $\sigma_s = 0.5$ (left panel) and different σ_s with $P_s = 0.4$ (right panel). Note that the vertical axis is on the log scale.

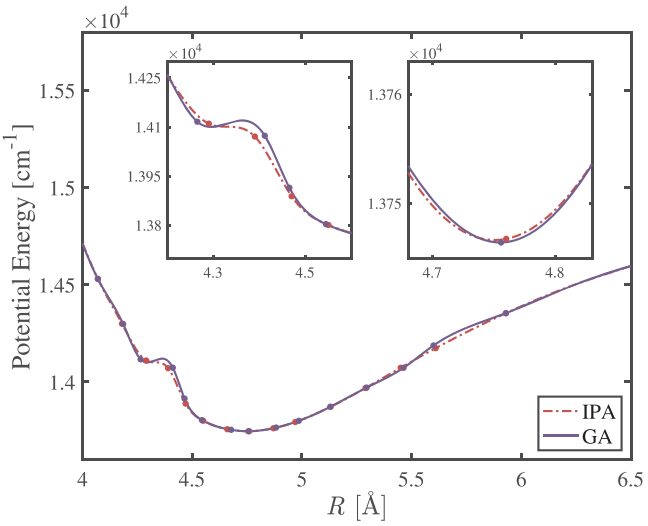

Figure 6. The PEC for $B^1\Pi$ state of $^{85}Rb^{133}Cs$ obtained by the GA (blue solid line) and by IPA [27] (red dot-dashed line). The subfigures are local zooms of the bump-like region and the bottom of the potential well.

the fitting, the fitted PEC describes the PAS more accurately as W increases. Therefore, when W increases, χ^2_{PA} decreases and χ^2_{FT} increases. As shown in figure 4, these two fitted lines intersect roughly at $W = 0.32$, and we set $W = 0.32$ in what follows.

Like the process above, we change P_m from 0.1 to 0.9 in a step length of 0.1, with other hyperparameters all fixed. According to the results of repeated trials, the value of χ^2_{FT} varies slightly with different P_m, while χ^2_{PA} is relatively smaller near $P_m = 0.3$. Meanwhile, we also try different values of P_c, and it seems to have little effect on both χ^2_{FT} and χ^2_{PA}. Consequently, we set $P_m = 0.3$ and $P_c = 0.4$ in the following. We then investigate the effect of P_s and σ_s on the fitting. We run our procedure as above for $P_s = 0.3, 0.5, 0.8$, initially, setting other hyperparameters to fixed values. Repeated trials show that our algorithm has almost always located the global minima when the iteration proceeds to 70%. Therefore, we reduce P_s by half during the remaining iterations to accelerate the descent to the global minima. We can get the best fitness value for each generation. Since we run 10 times for each setting of hyperparameters, we calculate the average of the best fitness values for these 10 runs. Then we calculate the square root of this average, noted as χ_{avg}. The variation of χ_{avg} as a function of generation number is shown in the left panel of figure 5. Meanwhile, we run our procedure for $\sigma_s = 0.5, 0.25, 0.125$ with other hyperparameters fixed and compute χ_{avg} for each generation, which is shown in the right panel of figure 5. The results for $P_s = 0.5$ and $\sigma_s = 0.25$ are relatively better than the others, as shown in figure 5.

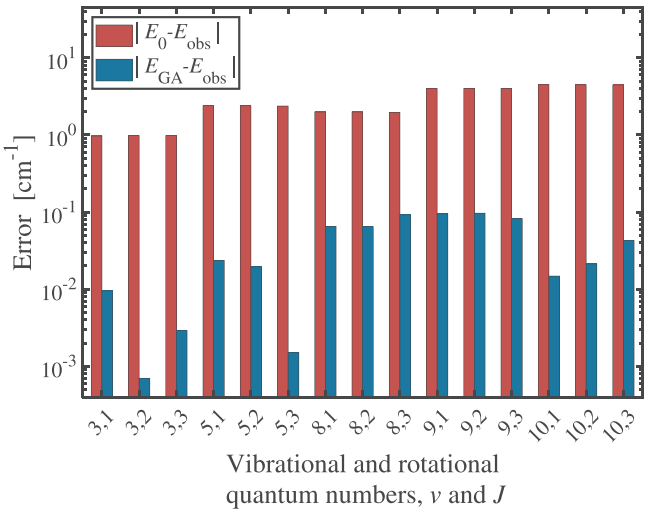

Figure 7. $|E_0 - E_{obs}|$ and $|E_{GA} - E_{obs}|$ for rovibrational levels observed by PAS. E_{obs} are energies of rovibrational levels observed by PAS in [10]. E_0 are energies calculated with the empirical PEC in [27]. E_{GA} are energies calculated by the PEC obtained in this work. For each set of quantum numbers, the left bar represents $|E_0 - E_{obs}|$, and the right bar represents $|E_{GA} - E_{obs}|$. Note that the vertical axis is on the log scale.

Table 2. Comparison of molecular constants in the present work with their counterparts obtained by IPA or *ab initio* calculations.

	Experiments		Theories			
	This work	IPA [27]	*ab initio* calculations [16–19]			
T_e [cm^{-1}]	13746.42	13746.65	13753	13743	13814	13750
ω_e [cm^{-1}]	41.06	39.4	38.62	40.8	35.04	37.0
R_e [Å]	4.755	4.751	4.676	4.616	4.72	4.79

After the exploration above, we determine the setting of hyperparameters used in the fitting: $W = 0.32$, $P_m = 0.3$, $P_c = 0.4$, $P_s = 0.5$, $\sigma_s = 0.25$. We run the procedure 10 times under the above setting and find the best one from the results. Then, we obtained the fitted PEC for $B^1\Pi$ state, which is shown in figure 6 together with the PEC obtained in [27]. It is worth noting that the bump-like region is more protruding, and the equilibrium internuclear distance R_e is slightly shifted to the right. The point-wise PEC data are listed in table 1. Additionally, we compare the molecular constants, including T_e, ω_e and R_e, with their counterparts obtained from the previous studies [16–19, 27], which are listed in table 2.

We also calculate the energies of rovibrational levels with the fitted PEC, which are denoted by E_{GA} and listed in tables A1, A2 and A3. The energies calculated with the PEC taken from [27] are also presented, which are denoted by E_0. As listed in these tables, our PEC can precisely reproduce the energy levels observed by both PAS and FTS. As shown in figure 7, $|E_{GA} - E_{obs}|$ is two orders of magnitude smaller than $|E_0 - E_{obs}|$ for rovibrational levels observed by PAS. Besides, we calculate the root mean square error (RMSE) between E_{cal} and E_{obs},

$$\mathrm{RMSE} = \frac{1}{N_c}\sqrt{\sum_{v,J}[E_{cal}(v, J) - E_{obs}(v, J)]^2}\,, \tag{6}$$

where E_{cal} stands for E_0 or E_{GA}, and N_c stands for N_{FT} or N_{PA}. After the optimisation of the present work, RMSE for energy levels observed by PAS is reduced from 3.055 cm^{-1} to 0.055 cm^{-1}. Meanwhile, RMSE for energy levels observed by FTS varies from 0.053 cm^{-1} to 0.051 cm^{-1}.

4. Conclusions

The present study was designed to fit the PEC for $B^1\Pi$ state of $^{85}Rb^{133}Cs$ via genetic algorithm, aiming to describe both FTS and PAS experimental data. We used a value-based scheme to encode the point-wise PECs into the individuals, which compose the population in GA. Our algorithm adopted the operators including tournament selection, simplified one-point crossover and improved non-uniform mutation, and it also employed the elitist preservation strategy after each generation. The evolutionary process was iterated for

200 generations with a population size of 200 individuals. We investigated the influence of hyperparameters on the iteration process and final results, and determined the setting of hyperparameters. Finally, we obtained the fitted PEC for $B^1\Pi$ state of $^{85}Rb^{133}Cs$. In comparison with the corresponding experimental data, the error of the rovibrational levels reproduced by the fitted PEC is less than 0.06 cm^{-1} on average.

The PEC in the present study features a bump-like region. To deal with this situation, we improved the encoding scheme by incorporating both horizontal and vertical coordinates of the potential points into the genes, so the PEC can exhibit a greater variety and flexibility. Additionally, such unusual shapes arise from the perturbation of neighboring electronic states due to spin–orbit coupling. To more accurately describe the observed perturbed data, a deperturbation analysis of the strongly coupled $B^1\Pi - c^3\Sigma^+$ system is needed, which necessitates more systematic spectroscopic data. Last but not least, we will apply the obtained PEC to simulate the photoassociation dynamics of $^{85}Rb^{133}Cs$ molecule in the future.

Acknowledgments

This work has been supported by National Natural Science Foundation of China (No.12104082, 12241409, 12074231, 12274272), the Innovation Program for Quantum Science and Technology (2021ZD0302100), and Program of the State Key Laboratory of Quantum Optics and Quantum Optics Devices (No.KF201814).

Data availability statement

All data that support the findings of this study are included within the article (and any supplementary files).

Appendix. The data of energy levels used in the fitting

Table A1. The rovibrational energies and errors for $B^1\Pi$ state of $^{85}Rb^{133}Cs$. E_{obs} are energies of rovibrational levels experimentally observed by PAS in [10]. E_0 are energies calculated with the empirical PEC in [27]. E_{GA} are energies calculated by the PEC obtained in this work. All energy values are in cm^{-1}.

v	J	E_{obs}	E_0	E_0-E_{obs}	E_{GA}	E_{GA}-E_{obs}
3	1	13 884.3574	13 883.3857	−0.9717	13 884.3669	0.0095
3	2	13 884.4232	13 883.4415	−0.9817	13 884.4225	−0.0007
3	3	13 884.5089	13 883.5251	−0.9838	13 884.5060	−0.0029
5	1	13 965.7021	13 963.3048	−2.3973	13 965.6785	−0.0236
5	2	13 965.7520	13 963.3592	−2.3928	13 965.7325	−0.0195
5	3	13 965.8150	13 963.4407	−2.3743	13 965.8135	−0.0015
8	1	14 080.6209	14 078.6305	−1.9904	14 080.6863	0.0654
8	2	14 080.6742	14 078.6837	−1.9905	14 080.7390	0.0648
8	3	14 080.7258	14 078.7636	−1.9622	14 080.8179	0.0921
9	1	14 117.2526	14 113.2392	−4.0134	14 117.1575	−0.0951
9	2	14 117.3080	14 113.2931	−4.0149	14 117.2112	−0.0968
9	3	14 117.3741	14 113.3739	−4.0002	14 117.2917	−0.0824
10	1	14 148.2887	14 143.8058	−4.4829	14 148.3035	0.0148
10	2	14 148.3398	14 143.8613	−4.4785	14 148.3611	0.0213
10	3	14 148.4047	14 143.9446	−4.4601	14 148.4476	0.0429

Table A2. The energies of rovibrational levels with $v = 0$ for $B^1\Pi$ state of $^{85}Rb^{133}Cs$ molecule. E_{obs} are energies of rovibrational levels experimentally observed by FTS in [27]. E_0 energies are calculated with the empirical PEC in [27]. E_{GA} are energies calculated by the PEC obtained in this work. All energy values are in cm^{-1}.

v	J	E_{obs}	E_0	E_0-E_{obs}	E_{GA}	E_{GA}-E_{obs}
0	25	13 775.4826	13 775.4678	−0.0148	13 775.4544	−0.0282
0	43	13 793.2945	13 793.2934	−0.0011	13 793.2808	−0.0137
0	44	13 794.5499	13 794.5555	0.0056	13 794.5429	−0.0070
0	46	13 797.1578	13 797.1653	0.0075	13 797.1529	−0.0049
0	47	13 798.5008	13 798.513	0.0122	13 798.5007	−0.0001
0	69	13 835.3102	13 835.3639	0.0537	13 835.3535	0.0433
0	70	13 837.3025	13 837.3652	0.0627	13 837.3549	0.0524
0	76	13 849.9378	13 849.9664	0.0286	13 849.9568	0.0190
0	82	13 863.6165	13 863.5824	−0.0341	13 863.5736	−0.0429
0	83	13 865.9762	13 865.9501	−0.0261	13 865.9415	−0.0347
0	90	13 883.3073	13 883.3098	0.0025	13 883.3022	−0.0051
0	91	13 885.8970	13 885.9018	0.0048	13 885.8943	−0.0027
0	92	13 888.5144	13 888.5217	0.0073	13 888.5144	0.0000
0	93	13 891.1622	13 891.1695	0.0073	13 891.1624	0.0002
0	94	13 893.8357	13 893.8452	0.0095	13 893.8383	0.0026
0	100	13 910.4668	13 910.4847	0.0179	13 910.4788	0.0120
0	101	13 913.3390	13 913.3553	0.0163	13 913.3496	0.0106
0	102	13 916.2341	13 916.2537	0.0196	13 916.2481	0.0140
0	103	13 919.1560	13 919.1798	0.0238	13 919.1744	0.0184
0	104	13 922.1095	13 922.1336	0.0241	13 922.1284	0.0189
0	115	13 956.4606	13 956.4491	−0.0115	13 956.4462	−0.0144
0	116	13 959.7357	13 959.7339	−0.0018	13 959.7312	−0.0045
0	119	13 969.7786	13 969.7528	−0.0258	13 969.7509	−0.0277
0	120	13 973.1538	13 973.1473	−0.0065	13 973.1456	−0.0082
0	121	13 976.5667	13 976.5690	0.0023	13 976.5676	0.0009

Table A3. The energies of rovibrational levels with $v = 1$ and $v = 2$ for $B^1\Pi$ state of $^{85}Rb^{133}Cs$ molecule. E_{obs} are energies of rovibrational levels experimentally observed by FTS in [27]. E_0 are energies calculated with the empirical PEC in [27]. E_{GA} are energies calculated by the PEC obtained in this work. All energy values are in cm^{-1}.

v	J	E_{obs}	E_0	E_0-E_{obs}	E_{GA}	E_{GA}-E_{obs}
1	32	13 819.8985	13 819.9439	0.0454	13 819.9649	0.0664
1	34	13 821.7896	13 821.8532	0.0636	13 821.8740	0.0844
1	73	13 881.8803	13 881.7317	−0.1486	13 881.7511	−0.1292
1	74	13 883.9664	13 883.8309	−0.1355	13 883.8503	−0.1161
1	75	13 886.0808	13 885.9581	−0.1227	13 885.9775	−0.1033
1	86	13 911.2072	13 911.2034	−0.0038	13 911.2230	0.0158
1	87	13 913.6599	13 913.6659	0.0060	13 913.6855	0.0256
1	88	13 916.1411	13 916.1562	0.0151	13 916.1758	0.0347
1	89	13 918.6494	13 918.6743	0.0249	13 918.6939	0.0445
1	90	13 921.1825	13 921.2202	0.0377	13 921.2399	0.0574
1	91	13 923.7427	13 923.7939	0.0512	13 923.8136	0.0709
1	111	13 981.1667	13 981.0743	−0.0924	13 981.0951	−0.0716
1	112	13 984.3011	13 984.2272	−0.0739	13 984.2480	−0.0531
1	113	13 987.4688	13 987.4074	−0.0614	13 987.4282	−0.0406
1	114	13 990.6578	13 990.6149	−0.0429	13 990.6358	−0.0220
1	125	14 027.6375	14 027.6953	0.0578	14 027.7166	0.0791
1	126	14 031.1531	14 031.2290	0.0759	14 031.2503	0.0972
1	138	14 075.8114	14 075.7343	−0.0771	14 075.7557	−0.0557
1	139	14 079.6671	14 079.6173	−0.0498	14 079.6387	−0.0284
1	140	14 083.5612	14 083.5270	−0.0342	14 083.5484	−0.0128
2	138	14 112.3627	14 112.2613	−0.1014	14 112.2970	−0.0657
2	139	14 116.1900	14 116.1136	−0.0764	14 116.1520	−0.0380
2	140	14 120.0433	14 119.9924	−0.0509	14 120.0336	−0.0097
2	141	14 123.9248	14 123.8978	−0.0270	14 123.9419	0.0171
2	144	14 135.7005	14 135.7727	0.0722	14 135.8262	0.1257

ORCID iDs

Yide Yin https://orcid.org/0009-0009-8151-1358
Yanting Zhao https://orcid.org/0000-0002-3343-2382
Gaoren Wang https://orcid.org/0000-0001-6216-7074

References

[1] Krems R, Friedrich B and Stwalley W C 2009 *Cold Molecules: Theory, Experiment, Applications* (CRC Press) (https://doi.org/10.1201/9781420059045)
[2] Ulmanis J, Deiglmayr J, Repp M, Wester R and Weidemueller M 2012 *Chem. Rev.* **112** 4890
[3] Chin C, Grimm R, Julienne P and Tiesinga E 2010 *Rev. Mod. Phys.* **82** 1225
[4] Ji Z 2012 Production and measurement of ultracold RbCs polar molecules *Ph.D. Thesis* Shanxi University
[5] Kerman A, Sage J, Sainis S, Bergeman T and DeMille D 2004 *Phys. Rev. Lett.* **92** 033004
[6] Gabbanini C and Dulieu O 2011 *Phys. Chem. Chem. Phys.* **13** 18905
[7] Bruzewicz C D, Gustavsson M, Shimasaki T and DeMille D 2014 *New J. Phys.* **16** 023018
[8] Shimasaki T, Bellos M, Bruzewicz C D, Lasner Z and DeMille D 2015 *Phys. Rev.* A **91** 021401
[9] Shimasaki T, Kim J T, Zhu Y and DeMille D 2018 *Phys. Rev.* A **98** 043423
[10] Liu Y, Gong T, Ji Z, Wang G, Zhao Y, Xiao L and Jia S 2019 *J. Chem. Phys.* **151** 084303
[11] Picard L R B *et al* 2023 *Phys. Rev. Res.* **5** 023149
[12] Hai Y, Li L, Li J, Wang G and Cong S 2020 *J. Chem. Phys.* **152** 174307
[13] Sun Z, Hai Y, Lyu B, Wang G and Cong S 2020 *J. Phys. B-At. Mol. Opt. Phys.* **53** 205204
[14] Yu Z, Si B, Sun Z, Lyu B and Cong S 2022 *J. Phys. B-At. Mol. Opt. Phys.* **55** 235201
[15] Pavolini D, Gustavsson T, Spiegelmann F and Daudey J 1989 *J. Phys. B-At. Mol. Opt. Phys.* **22** 1721
[16] Allouche A, Korek M, Fakherddin K, Chaalan A, Dagher M, Taher F and Aubert-Frecon M 2000 *J. Phys. B-At. Mol. Opt. Phys.* **33** 2307
[17] Fahs H, Allouche A, Korek M and Aubert-Frecon M 2002 *J. Phys. B-At. Mol. Opt. Phys.* **35** 1501
[18] Zaitsevskii A, Pazyuk E, Stolyarov A, Docenko O, Klincare I, Nikolayeva O, Auzinsh M, Tamanis M and Ferber R 2005 *Phys. Rev.* A **71** 012510
[19] Lim I S, Lee W C, Lee Y S and Jeung G H 2006 *J. Chem. Phys.* **124** 234307
[20] Rydberg R 1931 *Z. Phys.* **73** 376
[21] Klein O 1932 *Z. Phys.* **76** 226
[22] Rees A 1947 *Proc. Phys. Soc. Lond.* **59** 998
[23] Kirschner S and Watson J 1973 *J. Mol. Spectrosc.* **47** 234
[24] Le Roy R J 2017 *J. Quant. Spectrosc. Radiat. Transf.* **186** 158
[25] Kosman W and Hinze J 1975 *J. Mol. Spectrosc.* **56** 93
[26] Pashov A, Jastrzebski W and Kowalczyk P 2000 *Comput. Phys. Commun.* **128** 622
[27] Birzniece I, Docenko O, Nikolayeva O, Tamanis M and Ferber R 2013 *J. Chem. Phys.* **138** 154304
[28] Urbańczyk T and Koperski J 2018 *Spectroc. Acta Pt. A-Molec. Biomolec. Spectr.* **189** 502
[29] Ontaneda J, Vines F, Illas F and Grau-Crespo R 2019 *Phys. Chem. Chem. Phys.* **21** 10888
[30] Krosnicki M, Kedziorski A, Urbanczyk T and Koperski J 2019 *Phys. Rev.* A **99** 052510
[31] Urbańczyk T and Koperski J 2020 *Mol. Simul.* **46** 1073
[32] Sumpter B and Noid D 1992 *Chem. Phys. Lett.* **192** 455
[33] Khaliullin R Z, Eshet H, Kuehne T D, Behler J and Parrinello M 2010 *Phys. Rev.* B **81** 100103
[34] Coe J P 2019 *J. Chem. Theory Comput.* **15** 6179
[35] Roncaratti L F, Gargano R and Silva G M E 2006 *Theochem-J. Mol. Struct.* **769** 47
[36] Marques J M C, Prudente F V, Pereira F B, Almeida M M, Maniero A M and Fellows C E 2008 *J. Phys. B-At. Mol. Opt. Phys.* **41** 085103
[37] Almeida M M, Prudente F V, Fellows C E, Marques J M C and Pereira F B 2011 *J. Phys. B-At. Mol. Opt. Phys.* **44** 225102
[38] Stevenson I C 2020 Spectroscopy of ultracold lithium-rubidium molecules *Ph.D. Thesis* Purdue University
[39] Stevenson I C and Pérez-Ríos J 2019 *J. Phys. B-At. Mol. Opt. Phys.* **52** 105002
[40] Goldberg D E 1989 *Genetic Algorithms in Search, Optimization and Machine Learning* (Addison-Wesley Longman Publishing Co., Inc.) 1st edn
[41] Katoch S, Chauhan S S and Kumar V 2021 *Multimed. Tools Appl.* **80** 8091
[42] Le Roy R J 2017 *J. Quant. Spectrosc. Radiat. Transf.* **186** 167
[43] Xie H and Zhang M 2013 *IEEE Trans. Evol. Comput.* **17** 1
[44] Zhao X, Gao X S and Hu Z C 2007 *Appl. Math. Comput.* **192** 1